Nanoscale Advances

ROYAL SOCIETY OF CHEMISTRY

PAPER

View Article Online
View Journal | View Issue

Cite this: *Nanoscale Adv.*, 2023, **5**, 4892

Perfluoropentane/apatinib-encapsulated metal–organic framework nanoparticles enhanced the microwave ablation of hepatocellular carcinoma†

Dongyun Zhang,‡ Yixuan Zhang,‡ Yanchun Luo, Erpeng Qi, Jie Yu* and Ping Liang *

Received 2nd December 2022
Accepted 11th July 2023

DOI: 10.1039/d2na00880g

rsc.li/nanoscale-advances

Microwave ablation (MWA) is a promising minimally invasive therapy for hepatocellular carcinoma (HCC). However, the efficiency of MWA in treating HCC is evidently limited by the incomplete ablation of large tumors and tumors in high-risk locations. Here we designed an iron-based metal–organic framework nanomedicine (PFP-Apa-MOF) by loading perfluoropentane (PFP) and apatinib (Apa). After being absorbed by HCC, iron could induce ferroptosis. PFP could be activated into bubbles and act as an ultrasound agent for detecting the ablation margin. As an effective antiangiogenic drug, Apa could inhibit tumor residual growth after MWA. The high efficiency of PFP-Apa-MOF was fully demonstrated *in vitro* and *in vivo*. The results showed that MWA combined with PFP-Apa-MOF clearly enhanced the ablation efficiency, leading to apparent tumor inhibition, and increased tumor apoptosis and lipid peroxide. PFP-Apa-MOF could play a valuable role in enhancing MWA to achieve better therapeutic efficacy in HCC.

Introduction

Hepatocellular carcinoma (HCC) seriously threatens human health.[1] It ranks as the sixth most common form of cancer and the third leading cause of cancer-related death worldwide.[2] Microwave ablation (MWA) is a minimally invasive treatment method for early HCC, and it has attracted much attention from clinical doctors.[3] Compared with other thermal ablation methods, MWA exhibits better outcomes for HCC patients with tumors larger than 5 cm.[4] Despite being a promising minimally invasive treatment method for HCC, radical treatment of HCC is still difficult to achieve.[5] This is because of the limited ablation zone, the risk of thermal injury to adjacent visceral tissues, and metastasis adjacent to the ablation zone.[6] Hence, combination therapy is more advantageous than MWA alone. Therefore, there is an urgent need to find new strategies to improve the effectiveness of MWA.[7]

Qin *et al.* described that apatinib (Apa), an antiangiogenic agent, could serve as a control agent for HCC.[8] Apa is a small-molecule tyrosine kinase inhibitor that mainly targets vascular endothelial growth factor receptor-2 (VEGFR-2), which can strongly inhibit tumor neoangiogenesis. Apa also inhibits VEGFR-2-mediated downstream signaling, tumor growth, and metastasis.[9] However, Apa has many adverse effects, including drug-related adverse reactions and poor and limited accumulation in the tumor, which significantly restrict its application in patients with HCC.[10] With the rapid development of nanomedicine, the application of nanoparticles in antitumor therapy has attracted increasing attention, and nanomedicine has provided many new ideas for the diagnosis and treatment of tumors.[11] Nanoscale biomaterials rely on the enhanced permeability and retention (EPR) effect to accumulate in tumor tissues and become a good mediator for tumor imaging diagnosis and therapy.[12]

A metal–organic framework (MOF) is characterized by a molecular/atomic-level catalytic center and has the advantages of large surface area, high porosity, high loading capacity, and homogeneous structure.[13] In addition, MOF materials have good biosafety and biological degradation ability, so they have great application potential in medical tumor diagnosis and treatment.[14] In the synthesis of MOF materials, the self-assembly process of MOF materials can be regulated by regulating internal factors (metal ions, organic ligands, *etc.*) and external factors (synthesis method, reaction temperature, pH, *etc.*), so as to regulate their structure and performance.[15]

In the present study, we designed an iron-based MOF nanomedicine (PFP-Apa-MOF) by loading perfluoropentane (PFP) and Apa. Iron could induce ferroptosis after being absorbed by HCC, subsequently releasing iron ions in response to the weak acidity of lysosomes. PFP could be activated into bubbles after phase transformation by MWA. PFP-assisted ultrasound (US) contrast can be used to observe focal blood flow perfusion in real time to help control the ablation zone and provide guidance for MWA. Apa, an effective antiangiogenic drug, could inhibit tumor recurrence after MWA (as shown in Scheme 1). Owing to the multifunctional characteristics of PFP-Apa-MOF, we aim to

Department of Interventional Ultrasound, Fifth Medical Center of Chinese PLA General Hospital, Beijing, China. E-mail: jiemi301@163.com; liangping301@hotmail.com

† Electronic supplementary information (ESI) available. See DOI: https://doi.org/10.1039/d2na00880g

‡ Dongyun Zhang and Yixuan Zhang contributed equally to this work.

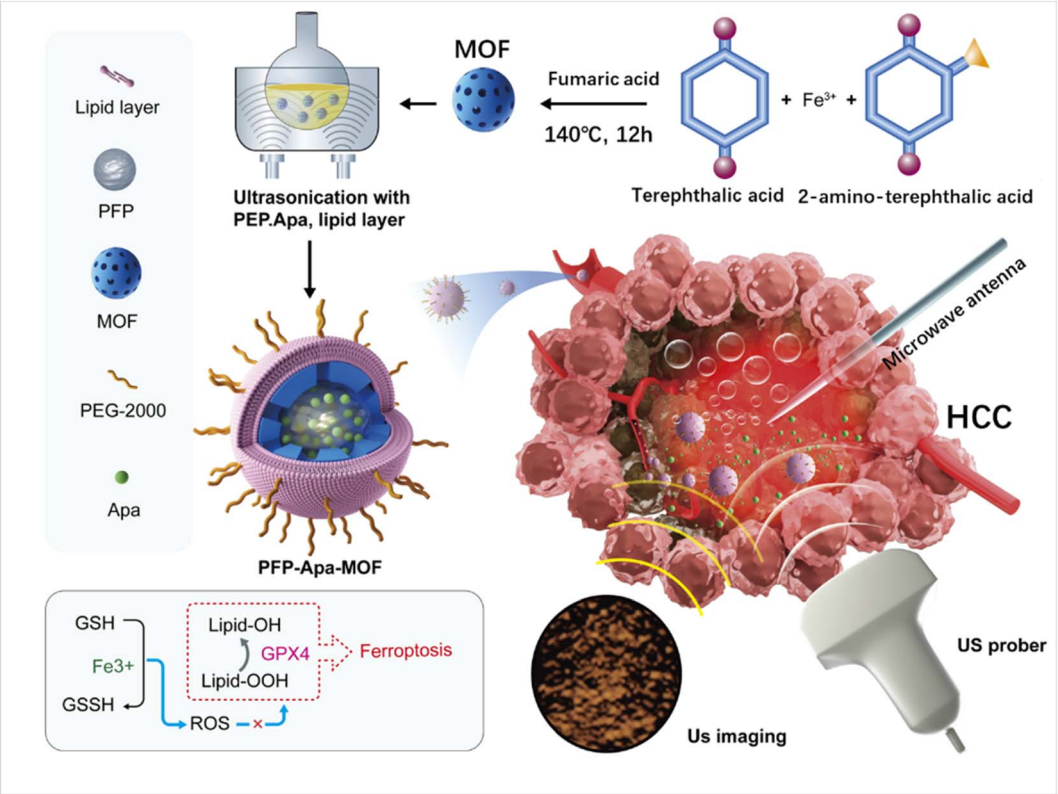

Scheme 1 Schematic illustration of perfluoropentane/apatinib-encapsulated metal–organic framework (PFP-Apa-MOF) as a theranostic agent for effective ultrasound imaging and enhanced microwave ablation (MWA) of hepatocellular carcinoma (HCC). PFP-Apa-MOF as a contrast agent for ultrasound imaging of HCC and coadjutant for ablation therapy. PFP is activated into bubbles after phase transformation by MWA. PFP-assisted ultrasound (US) contrast can be used to observe the ablation margin. Apa could inhibit tumor recurrence after MWA. Iron could increase the reactive oxygen species (ROS), and then ROS inhibits the function of GPX4 leading to tumor ferroptosis.

demonstrate that PFP-Apa-MOF can act as an excellent US agent for monitoring MWA and enhance its efficiency.

Materials and methods

Materials

N,*N*-Dimethylformamide (DMF), 1,2-dioleacyl-*sn*-propyl-3-choline phosphate (DOPC), 1,2-dioleacyl-*sn*-propyl-3-phosphatidyleth anolamine (DOPE), 1,2-distearoyl-*sn-glycero*-3-phosphoethanol-amine-*N*-[methoxy(poly-ethylene-glycol)-2000] (DSPE-PEG2000), DSPE-PEG2000-FITC, and cholesterol (CH) were purchased from Macklin (Shanghai, China). PFP was purchased from Strem Chemicals (MA, USA). Apa was purchased from Hengrui Pharmaceuticals (Jiangsu, China). Cell Counting Kit-8 (CCK-8), and Liperfluo Assay Kits were purchased from Dojindo Laboratories (Tokyo, Japan). Anti-GPX4 antibody and goat anti-rabbit antibody were purchased from Solarbio (Beijing, China). An Annexin V-FITC Apoptosis Kit was purchased from BioVision (USA).

Synthesis of PFP-Apa-MOF

PFP-Apa-MOF was synthesized as follows: first, an iron-based MOF was synthesized, and $FeCl_3 \cdot 6H_2O$ (3 mmol) was dissolved in 10 mL of DMF. Then, 10 mg of terephthalic acid, 5.2 mg of 2-aminoterephthalic acid, 10 mg of polyvinylpyrrolidone, and 87.1 mg of fumaric acid were added in the DMF mixture and refluxed at 140 °C for 12 h. The resultant solution was cooled to room temperature, and the solvent was evaporated. Then, the residue was precipitated in diethyl ethanol and washed with diethyl ether repeatedly. Second, 100 mg of DOPC, 5 mg of DOPE, 5 mg of DSPE-PEG2000, and 30 mg of CH were dissolved in 10 mL of chloroform. The organic solvent was removed under a nitrogen flow until a thin lipid film appeared. Third, an Apa-loaded MOF was synthesized. Five milliliters of 1 mg mL^{-1} Apa-ethanol, 5 mL of phosphate buffered saline (PBS), 3 mL of PFP, 60 mg of MOF, and the lipid film were mixed. The mixture was stirred for 24 h under dark conditions. The stirred dispersion of Apa-PFP-MOF was centrifuged at 12 000 g for 30 min and washed again with ethanol. The supernatant was measured for the Apa loading rate.

Characterization of PFP-Apa-MOF

Dynamic light scattering and stability measurements of nanoparticles were performed using a Zetasizer (Malvern Nano ZS, Melvin, UK), and each experiment was performed thrice. The morphology of PFP-Apa-MOF was further assessed by transmission electron microscopy (TEM) using a model HT7700 microscope (Hitachi, Tokyo, Japan). The MWA (1 W, 60 s) and

pH (8.0, 6.8, and 5.0) dependent release profiles of Apa were established by incubating PFP-Apa-MOF at room temperature, and the absorbance of the supernatant at 344 nm was measured at different time points with an ultraviolet spectrophotometer (UV1901PCS, Yoke Shanghai, China). For the H_2O_2 consumption levels of PFP-Apa-MOF, different concentrations of PFP-Apa-MOF were added in 200 μL of 3,3′,5,5′-tetramethylbenzidine (TMB) and incubated for 40 min. The reaction product was sampled at regular intervals and spectroscopically detected at 650 nm by using a Cytation™ 3 multiplate reader (Biotek, VT, USA). Each experiment was repeated six times.

Cytotoxicity caused by PFP-Apa-MOF

For more quantitative evaluation of the therapeutic efficacy of PFP-Apa-MOF, HepG2 cells were seeded into a 96-well plate (1×10^5 cells per well) at different concentrations of PFP-MOF and PFP-Apa-MOF for 24 h. The cell viability was assessed using CCK-8 detection kits, and the absorbance at 450 nm was measured using the multiplate reader. In this study, all experiments were designed for five repeating groups. To evaluate the combined cytotoxicity of PFP-Apa-MOF with MWA, 1×10^5 HepG2 cells were seeded in 96-well plates. In addition, 100 μL of fresh medium containing 5 μg mL^{-1} of Apa drug was added to each well, and the same concentration of free Apa was used as a parallel control. After 24 h, the cells were washed with PBS twice and changed with 250 μL of fresh medium. A microwave antenna was placed into the well, and cells were treated with MWA (1 W, 60 s), followed by cell viability assessment. Cells with different treatments as described above were collected. They were stained with the Annexin V-FITC/PI staining kit, and a flow cytometer (Cytoflex, Beckman Coulter, USA) was used to determine apoptosis/necrosis. We further investigated the generation of ROS in tumor cells using the multiplate reader. Cells were treated the same as in the cytotoxicity experiments, and cells were lysed and collected for centrifugation. The supernatant was measured at 560 nm absorbance.

Cellular invasion by transwell assay

The experiment above was repeated again, and cells were collected for examination of cellular invasion. Cells (1×10^5 cells per well) were seeded into an apical chamber. Afterward, 700 μL of culture medium containing 10% FBS was added. Transwell chambers were incubated for 24 h. The cells were washed twice with PBS and then fixed with 4% paraformaldehyde for 10 min. The cells were rinsed with PBS and stained with crystal violet for 10 min.

Lipid peroxide measurement using PFP-Apa-MOF

Liperfluo Assay Kits were used to detect the changes in lipid peroxides in HCC cells after PFP-Apa-MOF treatment. Fifty micrograms of Liperfluo were added to 60 μL of dimethyl sulfoxide, and then the mixture was added to RPMI 1640 medium to obtain Liperfluo solution at a concentration of 20 μmol L^{-1}. Cells were seeded in an 8-well μ-slide plate. Cells were treated the same as those in the cytotoxicity experiments, and they were collected and washed with PBS after different treatments. About 200 μL of Liperfluo solution was added to each well and incubated for 30 min in an incubator. Then, cells were collected for fluorescence imaging and flow cytometry.

Animal experiments

All animals in this study received care in accordance with the Guide for the Care and Use of Laboratory Animals published by the US National Institutes of Health. The experimental procedures were approved by the Chinese PLA General Hospital Animal Care and Use Committee. Female BALB/c nude mice (6–8 weeks old) were maintained under aseptic conditions in a small animal isolator and housed in groups of five in standard cages. All animals were allowed to adapt to the animal facility for at least seven days before the experiments. The HCC model was established by subcutaneously injecting 2×10^6 HepG2 cells into the right abdomen of mice.

$$\text{Tumor volume} = \text{length} \times (\text{width})^2/2$$

Synergistic therapy in the HCC model

For *in vivo* fluorescence imaging, 100 μL of FITC-PFP-Apa-MOF (containing 100 μg of MOF) was intravenously injected into tumor-bearing mice when the tumor size reached 10×10 mm. The fluorescence signals of FITC were obtained using an imaging spectrum system (LB983, Berthold, Germany; λ_{ex}: 490 nm; filter: 520 nm). Images at 1, 4, 10, and 24 h after FITC-PFP-Apa-MOF treatment were collected for further analysis. Each experiment was repeated three times. For tumor combination therapy, mice were divided into five groups (five mice per group), and each group was intravenously injected with 100 μL of PBS, PFP-Apa-MOF (containing 100 μg of MOF), and PFP-MOF (containing 100 μg of MOF). For the MWA treatment groups, the tumors of mice were treated with MWA 4 h later (1.0 W, 60 s). In addition, thermal images were recorded using an infrared thermal imaging camera. The tumor volume and change in the body weight of each mouse were recorded. The treatment above was repeated every five days. All mice were sacrificed on day 14 after the first treatment.

For the assessment of apoptosis, terminal deoxynucleotidyl transferase-mediated dUTP nick end labeling (TUNEL) was carried out with an *in situ* Cell Death Detection Kit according to the manufacturer's protocol. The cell apoptosis index was determined by calculating the percentage of positively stained cells for all cells from six randomly chosen fields/sections at 400× magnification. For the selenoenzyme glutathione peroxidase 4 (GPX4) experiments, the procedures were conducted according to the manufacturer's protocol. The fluorescence intensity of each image was calculated with ImageJ software. Blood was collected for blood biochemistry examination (Mindray BC-5130, China) and complete blood analysis (Roche cobas 8800, Switzerland). Tumors were collected for further analysis.

In vitro and *in vivo* US imaging

In vitro US images of PFP-Apa-MOF were acquired using an US instrument (ZS3 Exp, Mindray, China). About 5 mg mL^{-1} of Apa-

MOF and PFP-Apa-MOF were added into a 5 mL tube, and the same volume of PBS was used as the control. The solution was heated by MWA at 1 W. Infrared thermographic maps were obtained using an infrared thermal imaging camera (Magnity Electronics, Shanghai, China). US and light images of the solution were obtained after MWA. For *in vivo* imaging, 100 μL of PBS or PFP-Apa-MOF (containing 100 μg of MOF) was intravenously injected into a HepG2 tumor-bearing mouse. After 4 h, contrast-enhanced ultrasound imaging was conducted before and after MWA (1 W), and the tumor temperature was monitored with an infrared thermal imaging camera to obtain temperatures at 35 °C, 40 °C, and 45 °C. Each experiment was repeated three times. All the images were stored on hard drives for offline analysis.

Statistical analysis

The results of this study are presented as mean ± SD. Student's *t*-test was used to compare the cell viability. In addition, the tumor volume and weight, mouse body weight, and results of blood biochemistry examinations were compared using one-way ANOVA. The differences were considered statistically significant at $^{*}P < 0.05$, and they were very significant at $^{**}P < 0.001$ and $^{***}P < 0.0001$.

Results

Characterization of PFP-Apa-MOF

The procedure for the synthesis of PFP-Apa-MOF is illustrated in Scheme 1. Apa and PFP were encapsulated into the MOF. TEM revealed that PFP-Apa-MOF has a regular spherical shape (Fig. 1A). Dynamic light scattering revealed that PFP-Apa-MOF has good size distribution, and the hydrodynamic size was 386.6 ± 8.3 nm (Fig. 1B). TEM showed that the iron-based MOF had an obviously hollow structure and small particle size (293.3 ± 6.8 nm) (Fig. S1A and B†). The zeta potentials of the iron-based MOF and PFP-Apa-MOF were −28.4 ± 9.8 and −31.6 ± 10.6 mV (Fig. S1C†). PFP-Apa-MOF was coated with bistratal phospholipids to improve dispersity and biocompatibility. The encapsulation percentage of Apa was 69.7 ± 2.9%.

Apa release was performed to analyze the dependency of pH conditions on the release efficiency of PFP-Apa-MOF. The drug curve revealed that PFP-Apa-MOF showed the quickest release rate at pH 5.5 (Fig. 1C). The PFP-Apa-MOF showed good stability on different days (Fig. 1D). The drug release curve after MWA revealed that Apa was obviously released from PFP-Apa-MOF after MWA treatment (Fig. 1E). Peroxidase is a kind of enzyme used for digesting H_2O_2. Many MOF nanoparticles can catalyze the oxidation of TMB to generate blue reactions.[16] In this study, the peroxidase-like activity of PFP-Apa-MOF was evaluated through the catalytic reaction of TMB. The color of the TMB solution changed to blue after oxidation, and the degree of blue color was coincident with the concentration of PFP-Apa-MOF (Fig. S2†). The absorbance of the oxidation product of TMB exhibited a concentration- and time-dependent tendency with the concentration of PFP-Apa-MOF (Fig. 1F). These results proved that the colored products generated by the reaction of TMB were positively correlated with the PFP-Apa-MOF material. For the quantitative evaluation of PFP-Apa-MOF cytotoxicity, HepG2 cells were seeded into a 96-well plate at different concentrations of PFP-MOF and PFP-Apa-MOF for 24 h. The cell viability was assessed using the CCK-8 detection kit. PFP-Apa-MOF exhibited cellular suppression at a concentration of 10 μg mL^{-1}, whereas PFP-MOF exhibited slight cytotoxicity at a concentration of 50 μg mL^{-1}. The cytotoxicity of PFP-MOF and PFP-Apa-MOF was obviously increased at a concentration of 100 μg mL^{-1} (Fig. 1G).

Cytotoxicity therapy of PFP-Apa-MOF combined with MWA *in vitro*

The cell activity of PFP-Apa-MOF combined with MWA was evaluated. MWA alone produced slight cellular suppression at 1 W and 60 s, whereas nearly 50% of the cells were killed in the

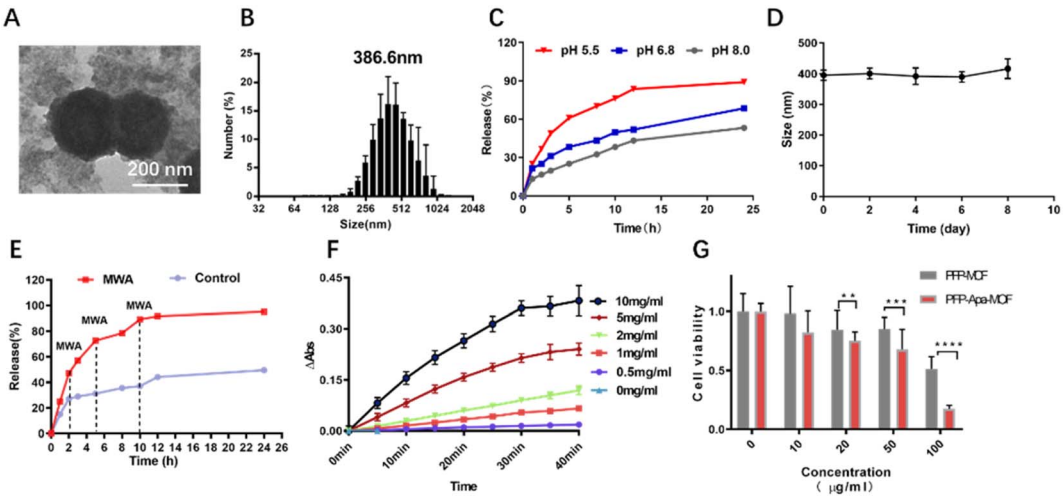

Fig. 1 Characterization of the PFP-Apa-MOF. (A) SEM of the PFP-Apa-MOF. (B) Particle number distribution of PFP-Apa-MOF. (C) Release curve of apatinib from PFP-Apa-MOF under different pH conditions. (D) The stability of PFP-Apa-MOF on different days. (E) Release curve of apatinib from PFP-Apa-MOF under MWA treatment. (F) Absorbance curve of TMB at different concentrations of PFP-Apa-MOF. (G) The viability of HepG2 cells incubated with PFP-MOF or PFP-Apa-MOF at different concentrations for 24 h. (Student's *t*-test was used, $^{*}P < 0.05$, $^{**}P < 0.001$ and $^{***}P < 0.0001$.)

PFP-MOF + MWA group (Fig. 2A). The combination of PFP-Apa-MOF with MWA induced 44.7 ± 1.8% cell death. The lethal effect of PFP-Apa-MOF + MWA was significantly higher than that of MWA + PFP-MOF, which corresponded with the cellular cytotoxicity results. Cell inhibition was not significantly different between the MWA and PFP-MOF + MWA groups (Fig. 2A). According to the results of transwell assay (Fig. 2B), the invasion and migration abilities of HCC cells in the MWA, PFP-MOF + MWA, and PFP-Apa-MOF + MWA groups were inhibited compared with the control group. Cells treated with Apa or PFP-Apa-MOF showed an obvious inhibition effect compared with the control group; however, the effect was obviously inferior compared with that of groups treated with MWA (Fig. 2B). The cytotoxic effect of PFP-Apa-MOF combined with MWA on HepG2 cells was further evaluated by flow cytometry. Cells were treated with PFP-Apa-MOF for 24 h with or without MWA and then labeled with PI and Annexin V. The PI+ Annexin V+ cells were defined as late apoptotic/necrotic cells. The results showed that PFP-Apa-MOF + MWA significantly induced more cell apoptosis/necrosis (34.0%) compared with MWA (8.8%) or PFP-Apa-MOF treatment alone (27.1%) (Fig. 2C). The results suggested that the cytotoxic effect of PFP-Apa-MOF on HCC cells could be enhanced by MWA treatment.

We further detected the ROS generation in cells. As shown in Fig. 2D, the ROS generation in PFP-Apa-MOF+MWA group generated the highest H_2O_2. Lipid peroxidation in HCC cells were tested using Liperfluo staining. Liperfluo signal significantly increased in the PFP-Apa-MOF+MWA group (Fig. 2E). Meanwhile, a reduction in lipid peroxidation was observed in cells treated with Apa or PFP-Apa-MOF. Flow cytometry revealed similar results with the fluorescent images (Fig. S3†). Quantitative analysis of flow cytometry showed that the lipid peroxidation in the PFP-Apa-MOF+MWA group was significantly different compared with that in the PFP-MOF+MWA group (Fig. 2F).

Synergistic therapy in the HCC model

Nanoparticle-based drugs could selectively accumulate into the tumor due to the EPR effect.[17] The amount of PFP-Apa-MOF that accumulated in the tumor was measured by fluorescence imaging. The fluorescence intensity of FITC-labeled PFP-Apa-MOF in the tumor increased gradually (Fig. S4A†). Continuous observation for 24 h revealed that the fluorescence intensity of PFP-Apa-MOF peaked at 4 h (Fig. S4B†). The schematic is presented in Fig. 3A. Mice were killed on day 14. The tumor volume and weight were recorded every two days. The tumor growth curve showed that tumors in the PFP-Apa-MOF group exhibited obvious differences compared with those in the control group, and the MWA group showed obviously better inhibition (Fig. 3B). The tumor growth in the PFP-MOF + MWA and PFP-Apa-MOF + MWA groups was significantly inhibited. However, the tumor growth in the PFP-Apa-MOF + MWA group was more significantly inhibited compared with that in the PFP-MOF + MWA group (Fig. 3B). There were no obvious weight changes in different groups after the treatment (Fig. S5†).

Mice in different groups were sacrificed at day 11. The tumor tissues of each group were removed, embedded in paraffin, sectioned, and stained with TUNEL and GPX4 to observe tumor apoptosis and ferroptosis. TUNEL staining showed that there

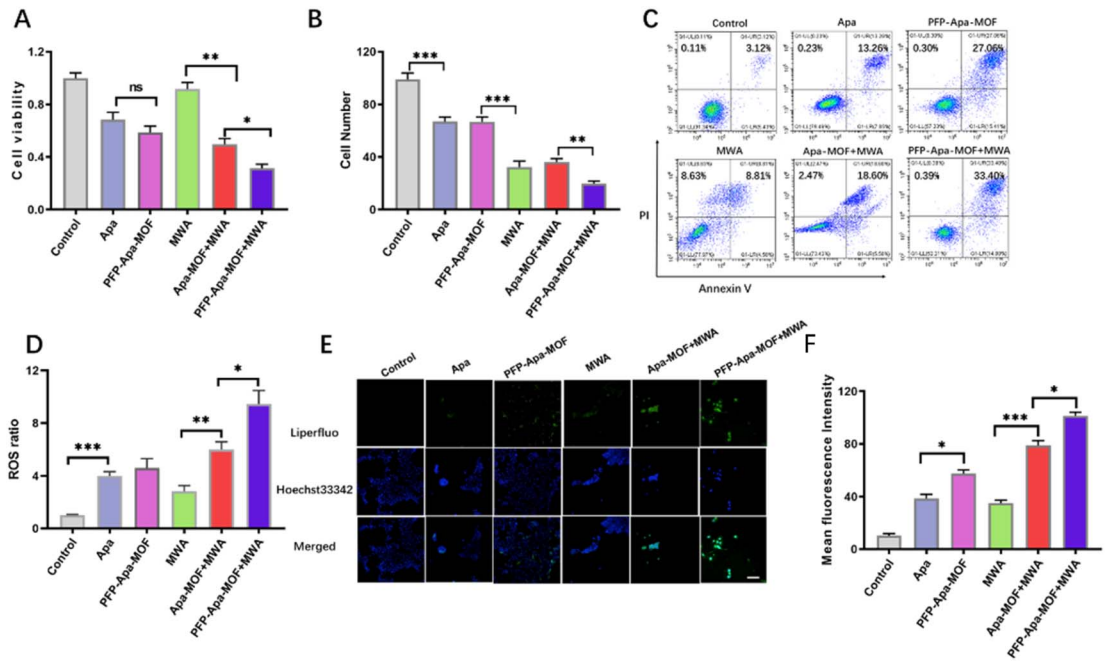

Fig. 2 *In vitro* cellular cytotoxicity, transwell assay, flow cytometry, lipid peroxidation of PFP-Apa-MOF combined MWA. (A) Cellular viability of different treatment. (B) Cell number of PFP-Apa-MOF combined MWA treatment after in transwell assay of different treatment. (C) Apoptotic and necrotic cells of different treatment by flow cytometry. (D) ROS generation *in vitro*. (E) Fluorescent staining of lipid peroxidation in different groups (scale bar: 100 μm). (F) Quantitative fluorescent staining of lipid peroxidation in different groups. (Student's *t*-test was used, ns: not significant, $*P < 0.05$, $**P < 0.001$ and $***P < 0.0001$).

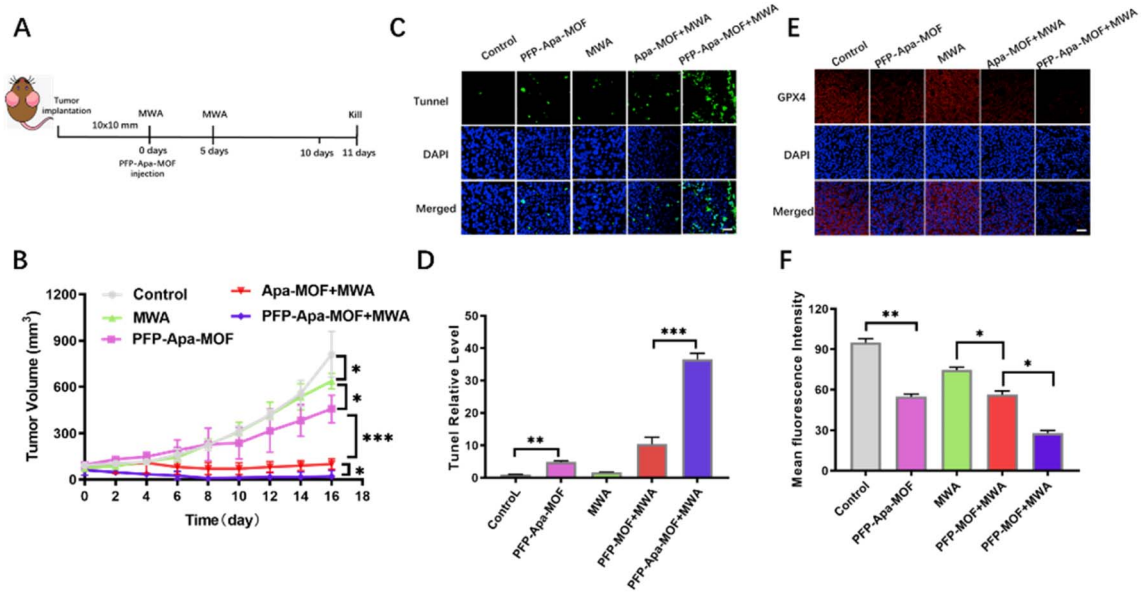

Fig. 3 *In vivo* antitumor effect of PFP-Apa-MOF combined MWA in HCC. (A) Schematic illustration of PFP-Apa-MOF combined MWA to inhibit tumor growth. (B) Tumor growth curves of five groups of mice (five mice per group). (C) TUNEL staining of tumors in the five groups (scale bar: 100 μm). (D) The quantitative apoptotic index of the TUNEL experiment. (E) GPX4 staining in tumors in the five groups (scale bar: 100 μm). (F) Quantitative fluorescence intensity of GPX4 in tumors. (Student's *t*-test was used, ns: not significant, $^{*}P < 0.05$, $^{**}P < 0.001$ and $^{***}P < 0.0001$.)

was apparent cell apoptosis in the control group and only relatively few apoptotic events in the MWA and PFP-Apa-MOF groups. Cell apoptosis was significantly increased in the PFP-MOF + MWA group, and the PFP-Apa-MOF + MWA group presented the highest amount of apoptosis (Fig. 3C). Quantitative analysis of apoptosis revealed 6.13 ± 0.77% and 3.85 ± 0.67% apoptotic cells in tumors treated with MWA and PFP-Apa-MOF. There were 13.55 ± 3.69% and 35.80 ± 4.09% apoptotic cells in the PFP-MOF + MWA and PFP-Apa-MOF + MWA groups, respectively (Fig. 3D). The amount of cell apoptosis significantly increased in the PFP-MOF + MWA and PFP-Apa-MOF + MWA groups (Fig. 3D). Ferroptosis is an iron-dependent form of necrotic cell death marked by oxidative damage to phospholipids. To date, phospholipid hydroperoxide-reducing enzyme GPX4 has been able to reduce toxic lipid peroxide to nontoxic hydroxyl compounds.[18] Thus, it is important to control ferroptosis.[19] The GPX4 experiments provided evidence that the fluorescence intensity of GPX4 was obviously decreased in tumor tissue compared with the control group (Fig. 4E). The fluorescence was significantly attenuated in the PFP-Apa-MOF, PFP-MOF + MWA, and PFP-Apa-MOF + MWA groups (Fig. 3E). Quantitative analysis revealed that the fluorescence intensity of PFP-Apa-MOF and PFP-MOF + MWA groups could induce some degree of ferroptosis and that both groups showed decreased fluorescence intensity (Fig. 3F). However, the fluorescence intensity in the PFP-Apa-MOF + MWA group was the lowest among the five groups (Fig. 3F).

Imaging performance of PFP-Apa-MOF

The US imaging properties of PFP-MOF and PFP-Apa-MOF were investigated in contrast mode with or without MWA. As shown in Fig. 4A, no macro-bubbles were observed at room temperature, whereas few macro-bubbles were observed at 40 °C. There were obviously more macro-bubbles at 45 °C than at 40 °C. However, there were no obvious macro-bubbles in the liposome-encapsulated PFP. Quantitative analysis of each scan showed that there were obvious differences in macro-bubbles between temperature at 40 °C and temperature at 45 °C (Fig. 4B). Because MWA triggered the liquid–gas phase transition of PFP, the US signal intensity of PFP-Apa-MOF differed significantly before and after MWA in contrast mode, indicating the superior capability of PFP-Apa-MOF in US imaging (Fig. 4C and D). Mice burdened with HCC tumors were injected with PFP-Apa-MOF *via* the tail vein. Four hours after the injection, MWA was performed to increase the local temperature to 45 °C, which could lead to micro-bubble formation. Therefore, a significant increase in the US signal was observed (Fig. 4E). The quantitative intensity of the US signal revealed obvious, significant differences between temperature at 40 °C and temperature at 45 °C; however, no difference was observed between temperature at 45 °C and temperature at 50 °C (Fig. 4F). The *in vivo* imaging results further demonstrated that PFP-Apa-MOF could be used as an efficient US agent to monitor the sublethal ablation margin.

In vivo toxicology analysis

The toxicity associated with each treatment was investigated *via in vivo* blood biochemistry tests. As shown in Fig. 5, the control, MWA, PFP-Apa-MOF, PFP-MOF + MWA, and PFP-Apa-MOF + MWA groups showed no significant toxicology. No significant abnormalities in alanine aminotransferase, albumin, total bilirubin, amylase, blood urea nitrogen, and creatinine were

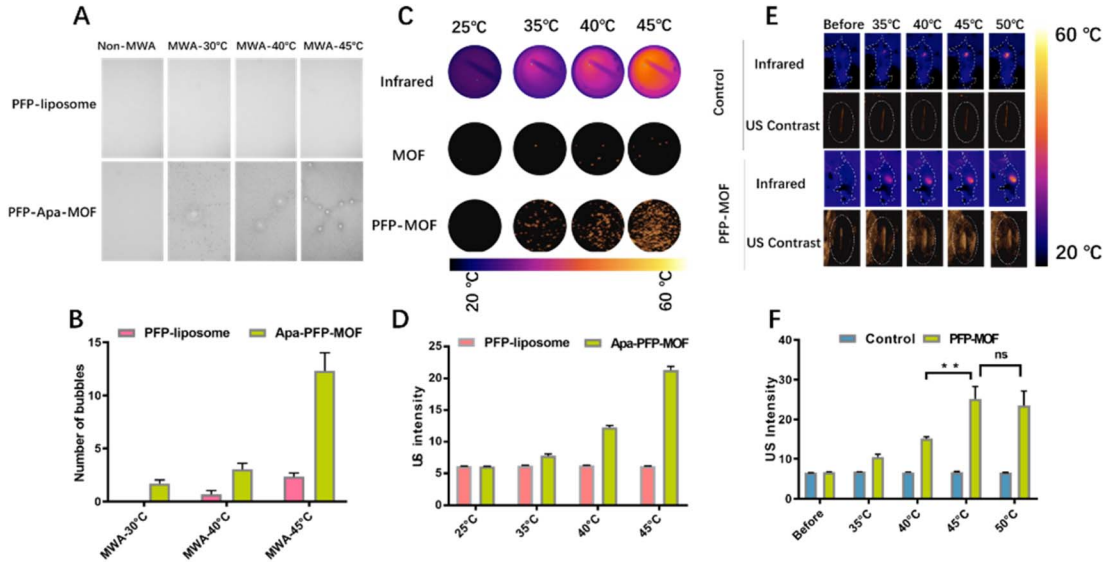

Fig. 4 Ultrasound (US) images in contrast-mode of PFP-Apa-MOF before and after MWA. (A) Macro-bubble formation of PFP-liposome and PFP-Apa-MOF at different temperatures under MWA conditions. (B) Quantitative macro-bubble formation in PFP-liposome and PFP-Apa-MOF. (C) Near-infrared image and US contrast intensity of PFP-liposome and PFP-Apa-MOF *in vitro*. (D) Quantitative US intensity of PFP-liposome and PFP-Apa-MOF. (E) Near-infrared image and US contrast intensity PFP-Apa-MOF *in vivo*. (F) Quantitative US intensity of PFP-Apa-MOF in tumors. (Student's *t*-test was used, ns: not significant,*$P < 0.05$, **$P < 0.001$ and ***$P < 0.0001$.)

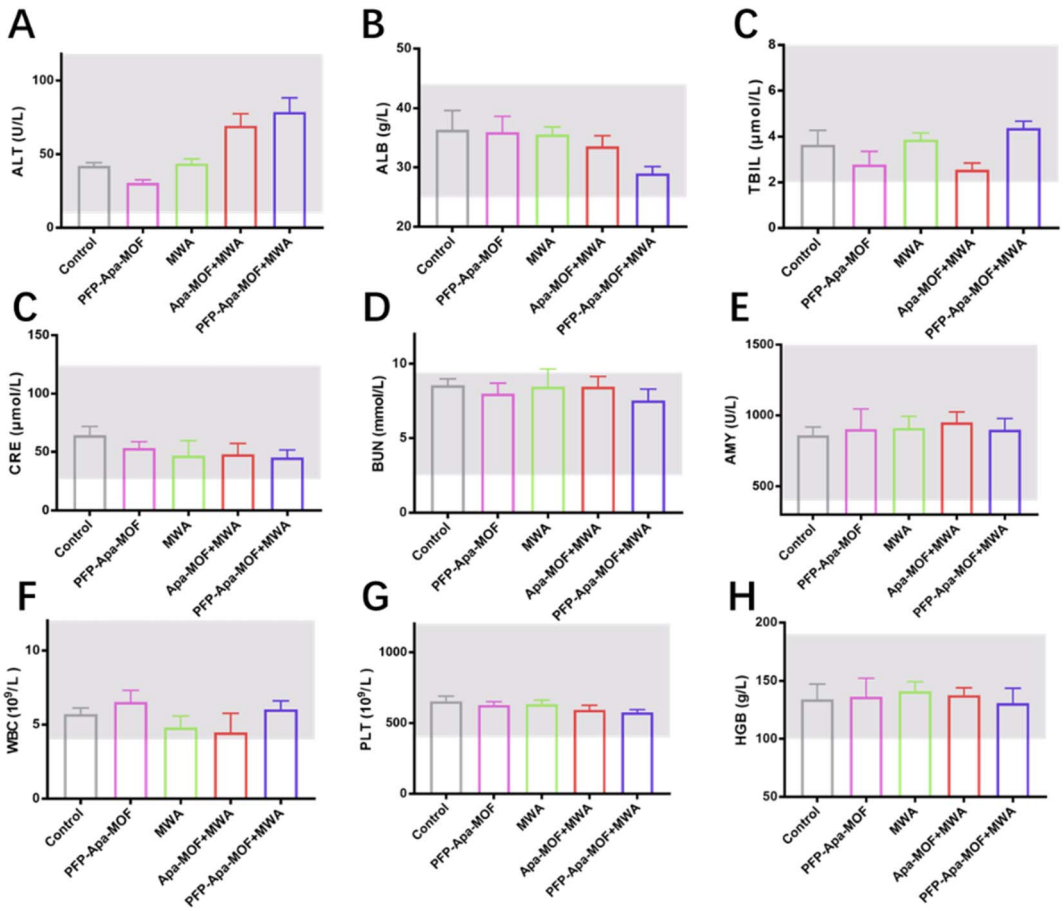

Fig. 5 Systematic toxicology evaluation of PFP-Apa-MOF combined MWA in HCC. (A–E) represent the serum biochemistry of ALT, ALB, TBIL, CRE, BUN, and AMY. (F–H) Hematological measurements of WBC, PLT, and HGB. (Gray zone represents the normal interval.)

observed. The mean values of hemoglobin, white blood cells, and platelets were within the normal range. Furthermore, the major organs of mice treated with liposomes packed with sodium chloride showed no noticeable damage or inflammation on HE staining among the five groups (Fig. S6†).

Discussion

MWA is a popular method used to treat HCC with considerable data confirming its safety and efficacy.[5] For tumors less than 5 cm, MWA has obtained similar outcomes to hepatic resection.[20] However, for tumors larger than 5 cm, achieving complete ablation is relatively difficult. Numerous technological improvements in MWA have been made in the past few decades to improve the prognosis of patients with HCC.[21] In this study, we designed iron-based MOF nanomaterials capable of loading PFP and Apa. PFP could act as an US contrast agent to achieve contrast imaging under microwave energy excitation, which could effectively monitor the thermal ablation field and identify the remaining HCC.[22] Apa, an antitumor neoangiogenic drug, is combined with PFP to enhance the MWA outcome.

MOF-based nanoparticles have been designed and studied for tumor therapy. An MOF possesses the following advantages: first, its smart structure endows the MOF with diverse compositions, sizes, and multifunctions; second, high porosities endow the MOF with high drug loading capacity; third, MOF is biodegradable due to its weak coordination bonds.[23] These advantages enable the MOF nanoparticle to become a promising carrier for tumor therapy.[24] In this study, we synthesized an iron-based MOF nanomedicine (PFP-Apa-MOF) by loading PFP and Apa. The MOF has a hollow structure to load the drug and induce ferroptosis. The MOF could inhibit the activity of GPX4, which decomposes lipid peroxide in the body. Thus, lipid peroxides in the tumor are increased after MOF treatment. Our results revealed that GPX4 was significantly decreased in the PFP-Apa-MOF, PFP-MOF + MWA, and PFP-Apa-MOF + MWA groups. Quantitative analysis revealed that the PFP-Apa-MOF + MWA group showed the lowest fluorescence intensity of GPX4 among the groups.

The exploration of nanoparticles as efficient drugs has attracted much interest and encouraged the translation of nanomedicine into clinical application.[25] An MOF has excellent biocompatibility and can overcome the problems of drug insolubility and instability.[26] Apa is insoluble in water; hence, the nanoparticle encapsulation of liposoluble drugs is usually high.[27] Our results showed that Apa was released from PFP-Apa-MOF after being triggered by MWA and was stable with MWA treatment. In this situation, Apa was released in the tumor, and precise control was realized. Moderate heat (45 °C) could stimulate the liquid–gas phase transition of PFP, which could strengthen the ablation margin. The ablation margin is known to be vital during ultrasound-guided MWA. Moreover, the phase transition of PFP enhances drug release.

Conclusion

In the present study, we describe a multifunctional nanoplatform of MOF loaded with PFP and Apa (PFP-Apa-MOF), showing good performance for MWA of HCC. The combination therapy appears to have substantial antitumor efficacy in HCC therapy. PFP-Apa-MOF can induce lipid peroxide and ferroptosis for effective tumor treatment. Moreover, PFP can be generated into micro-bubbles, enabling US imaging and enhancing the release of Apa. In addition, PFP-Apa-MOF possesses good biocompatibility and is nontoxic, indicating that PFP-Apa-MOF has promising potential for further clinical exploration.

Conflicts of interest

All authors declare no competing interests.

Acknowledgements

This work was supported by the National Scientific Foundation Committee of China (92159305 and 82030047).

References

1 K. Leuchte, E. Staib, M. Thelen, P. Gödel, A. Lechner, P. Zentis, M. Garcia-Marquez, D. Waldschmidt, R. R. Datta, R. Wahba, C. Wybranski, T. Zander, A. Quaas, U. Drebber, D. L. Stippel, C. Bruns, M. von Bergwelt-Baildon, K. Wennhold and H. A. Schlößer, *Cancer Immunol., Immunother.*, 2021, **70**(4), 893–907.

2 Z. Wang, M. Liu, D. Z. Zhang, S. S. Wu, Z. X. Hong, G. B. He, H. Yang, B. D. Xiang, X. Li, T. A. Jiang, K. Li, Z. Tang, F. Huang, M. Lu, J. A. Chen, Y. C. Lin, X. Lu, Y. Q. Wu, X. W. Zhang, Y. F. Zhang, C. Cheng, H. L. Ye, L. T. Wang, H. G. Zhong, J. H. Zhong, L. Wang, M. Chen, F. F. Liang, Y. Chen, Y. S. Xu, X. L. Yu, Z. G. Cheng, F. Y. Liu, Z. Y. Han, W. Z. Tang, J. Yu and P. Liang, *Hepatology*, 2022, **76**(1), 66–77.

3 (*a*) J. Yu, X. L. Yu, Z. Y. Han, Z. G. Cheng, F. Y. Liu, H. Y. Zhai, M. J. Mu, Y. M. Liu and P. Liang, *Gut*, 2017, **66**(6), 1172–1173; (*b*) P. Liang, B. Dong, X. Yu, D. Yu, Y. Wang, L. Feng and Q. Xiao, *Radiology*, 2005, **235**(1), 299–307; (*c*) F. Izzo, V. Granata, R. Grassi, R. Fusco, R. Palaia, P. Delrio, G. Carrafiello, D. Azoulay, A. Petrillo and S. A. Curley, *Oncologist*, 2019, **24**(10), e990–e1005.

4 H. Ren, C. An, P. Liang, J. Yu, Z. Cheng, Z. Han, F. Liu, L. Dong and D. Li, *Int. J. Hyperthermia*, 2019, **36**(1), 44–54.

5 N. Vietti Violi, R. Duran, B. Guiu, J. P. Cercueil, C. Aubé, A. Digklia, I. Pache, P. Deltenre, J. F. Knebel and A. Denys, *Lancet Gastroenterol. Hepatol.*, 2018, **3**(5), 317–325.

6 Y. X. Zhang, X. H. Zhang, X. L. Yu, Z. Y. Han, J. Yu, F. Y. Liu, Z. G. Cheng and P. Liang, *Int. J. Hyperthermia*, 2020, **37**(1), 688–695.

7 K. Wang, C. Wang, H. Jiang, Y. Zhang, W. Lin, J. Mo and C. Jin, *Front. Immunol.*, 2021, **12**, 792781.

8 S. Qin, Q. Li, S. Gu, X. Chen, L. Lin, Z. Wang, A. Xu, X. Chen, C. Zhou, Z. Ren, L. Yang, L. Xu, Y. Bai, L. Chen, J. Li, H. Pan, B. Cao, W. Fang, W. Wu, G. Wang, Y. Cheng, Z. Yu, X. Zhu, D. Jiang, Y. Lu, H. Wang, J. Xu, L. Bai, Y. Liu, H. Lin, C. Wu, Y. Zhang, P. Yan, C. Jin and J. Zou, *Lancet Gastroenterol. Hepatol.*, 2021, **6**(7), 559–568.

9 J. Xu, J. Shen, S. Gu, Y. Zhang, L. Wu, J. Wu, G. Shao, Y. Zhang, L. Xu, T. Yin, J. Liu, Z. Ren, J. Xiong, X. Mao, L. Zhang, J. Yang, L. Li, X. Chen, Z. Wang, K. Gu, X. Chen, Z. Pan, K. Ma, X. Zhou, Z. Yu, E. Li, G. Yin, X. Zhang, S. Wang and Q. Wang, *Clin. Cancer Res.*, 2021, **27**(4), 1003–1011.

10 J. E. Lee, K. L. Kim, D. Kim, Y. Yeo, H. Han, M. G. Kim, S. H. Kim, H. Kim, J. H. Jeong and W. Suh, *Int. J. Nanomed.*, 2017, **12**, 4813–4822.

11 (*a*) S. Wang, L. Zhang, J. Zhao, M. He, Y. Huang and S. Zhao, *Sci. Adv.*, 2021, **7**(12), 1–11; (*b*) Z. Ren, X. Chen, L. Hong, X. Zhao, G. Cui, A. Li, Y. Liu, L. Zhou, R. Sun, S. Shen, J. Li, J. Lou, H. Zhou, J. Wang, G. Xu, Z. Yu, Y. Song and X. Chen, *Small*, 2020, **16**(2), e1905233.

12 T. Zhou, X. Liang, P. Wang, Y. Hu, Y. Qi, Y. Jin, Y. Du, C. Fang and J. Tian, *ACS Nano*, 2020, **14**(10), 12679–12696.

13 S. Wang, C. M. McGuirk, A. d'Aquino, J. A. Mason and C. A. Mirkin, *Adv. Mater.*, 2018, **30**(37), e1800202.

14 W. Liang, P. Wied, F. Carraro, C. J. Sumby, B. Nidetzky, C. K. Tsung, P. Falcaro and C. J. Doonan, *Chem. Rev.*, 2021, **121**(3), 1077–1129.

15 C. Chu, M. Su, J. Zhu, D. Li, H. Cheng, X. Chen and G. Liu, *Theranostics*, 2019, **9**(11), 3134–3149.

16 H. Yu, H. Wu, X. Tian, Y. Zhou, C. Ren and Z. Wang, *RSC Adv.*, 2021, **11**(43), 26963–26973.

17 W. M. MacCuaig, B. L. Fouts, M. W. McNally, W. E. Grizzle, P. Chuong, A. Samykutty, P. Mukherjee, M. Li, J. B. Jasinski, B. Behkam and L. R. McNally, *ACS Appl. Mater. Interfaces*, 2021, **13**(42), 49614–49630.

18 D. Yang, Z. Liang, P. Tang, C. Zhang, M. Tang, Q. Li, J. J. Biendicho, J. Li, M. Heggen, R. E. Dunin-Borkowski, M. Xu, J. Llorca, J. Arbiol, J. R. Morante, S. L. Chou and A. Cabot, *Adv. Mater.*, 2022, **34**(10), e2108835.

19 S. Doll, F. P. Freitas, R. Shah, M. Aldrovandi, M. C. da Silva, I. Ingold, A. Goya Grocin, T. N. Xavier da Silva, E. Panzilius, C. H. Scheel, A. Mourão, K. Buday, M. Sato, J. Wanninger, T. Vignane, V. Mohana, M. Rehberg, A. Flatley, A. Schepers, A. Kurz, D. White, M. Sauer, M. Sattler, E. W. Tate, W. Schmitz, A. Schulze, V. O'Donnell, B. Proneth, G. M. Popowicz, D. A. Pratt, J. P. F. Angeli and M. Conrad, *Nature*, 2019, **575**(7784), 693–698.

20 H. Hu, J. C. Chi, R. Liu and B. Zhai, *Int. J. Hyperthermia*, 2021, **38**(1), 191–201.

21 Y. Feng, L. Wang, H. Lv, T. Shi, C. Xu, H. Zheng, J. Qi, X. Zhao, J. Li, Y. Gao, C. Qin and Q. Zhu, *HPB*, 2021, **23**(4), 512–519.

22 W. Dong, A. Huang, J. Huang, P. Wu, S. Guo, H. Liu, M. Qin, X. Yang, B. Zhang, M. Wan and Y. Zong, *Biomater. Sci.*, 2020, **8**(19), 5329–5345.

23 K. Li, C. Lin, M. Li, K. Xu, Y. He, Y. Mao, L. Lu, W. Geng, X. Li, Z. Luo and K. Cai, *ACS Nano*, 2022, **16**(2), 2381–2398.

24 Y. Li, J. Zhou, L. Wang and Z. Xie, *ACS Appl. Mater. Interfaces*, 2020, **12**(27), 30213–30220.

25 C. Zhang, L. Xin, J. Li, J. Cao, Y. Sun, X. Wang, J. Luo, Y. Zeng, Q. Li, Y. Zhang, T. Zhang and P. Huang, *Adv. Healthcare Mater.*, 2022, **11**(2), e2101946.

26 D. Wang, D. Jana and Y. Zhao, *Acc. Chem. Res.*, 2020, **53**(7), 1389–1400.

27 J. Liao, H. Jin, S. Li, L. Xu, Z. Peng, G. Wei, J. Long, Y. Guo, M. Kuang, Q. Zhou and S. Peng, *J. Exp. Clin. Cancer Res.*, 2019, **38**(1), 454.